Sensors and Materials, Vol. 34, No. 2 (2022) 595–602
MYU Tokyo

S & M 2831

Growth, Optical, and Scintillation Properties of $(Gd_{0.4}Lu_{0.6})_8Sr_2(SiO_4)_6O_2$ Crystals

Takayuki Yanagida,* Takumi Kato, Daisuke Nakauchi, and Noriaki Kawaguchi

Nara Institute of Science and Technology (NAIST), 8916-5, Takayama-cho, Ikoma-shi, Nara 630-0192, Japan

(Received October 9, 2021; accepted October 27, 2021)

Keywords: scintillator, crystal, apatite, ionizing radiation, scintillation detector

Non-doped and 0.1, 0.5, 1.0, and 2.0% Ce-doped $(Gd_{0.4}Lu_{0.6})_8Sr_2(SiO_4)_6O_2$ crystals were prepared and their optical and scintillation properties were investigated. Their X-ray diffraction (XRD) patterns confirmed that the Ce-doped samples did not contain an impurity phase, whereas the non-doped one contained some impurity phases such as Gd_2SiO_5 and Lu_2SiO_5. The emission due to 5d–4f transitions of Ce^{3+} was observed at 380–650 nm in both the photoluminescence (PL) and scintillation spectra of the Ce-doped samples. The scintillation light yields (*LY*s) of the 0.5 and 1.0% Ce-doped samples under ^{241}Am α-ray irradiation were ~230 and ~620 ph/5.5 MeV-α, respectively.

1. Introduction

Scintillators are one of the phosphor materials that show ionizing-radiation-induced luminescence (scintillation) when they absorb the energy of ionizing radiation.[1–3] Scintillators are generally combined with photodetectors such as a photomultiplier tube (PMT) and a Si photodiode, and such sensors are called scintillation detectors.[4] When compared with semiconductor detectors,[5–8] which are also common ionizing radiation detectors, scintillation detectors have some advantages especially in terms of detection efficiency and response speed. Owing to such properties, scintillation detectors are used in medicine,[9] security,[10] environmental monitoring,[11] biology,[12] resource extrapolation,[13] and high-energy physics.[14]

Scintillators are roughly classified into two types, namely, host emission type and emission-center-doped type. In the former, the host matrix itself has functions of ionizing radiation absorption and emission, the intensity of which is proportional to the absorbed energy. In host-emission-type scintillators, common materials are semiconductor scintillators[15–20] and some others.[21–26] In the latter, the functionalities of absorption and emission are assigned to the host and emission center, respectively.[27] The recent trend of R&D is on the former type, and preferable emission centers are Ce^{3+},[28–34] Pr^{3+},[35–38] some rare-earth ions,[39–51] and other ions that have electron transitions associated with luminescence.[52–57] The attraction to the emission-center-doped scintillators is explained by the controllability of emission wavelength and decay time, and among such emission center ions, Ce^{3+} is the most attractive owing to a good match of the emission wavelength with common PMTs, a fast decay time of typically several tens to

*Corresponding author: e-mail: t-yanagida@ms.naist.jp
https://doi.org/10.18494/SAM3684

ISSN 0914-4935
https://myukk.org/

hundreds of nanoseconds, and a relatively high probability to achieve a high scintillation light yield (*LY*). As is well known, conventional models[58–61] cannot predict *LY* but can only explain the observed *LY*; thus, empirical evidence of a high *LY* by the Ce^{3+} emission center is quite important in this field.

In this study, we have focused on a Ce-doped rare-earth apatite scintillator, the chemical composition of which can be expressed as $RE_8AE_2(SiO_4)_6O_2$, where RE and AE denote rare-earth and alkaline-earth metal elements, respectively. To date, we have studied a series of materials,[62–66] and among these materials, 0.5% Ce-doped $(Gd_{0.4}Lu_{0.6})_8Sr_2(SiO_4)_6O_2$ has shown the best *LY* with a high effective atomic number of 60.5. However, the optimum Ce concentration is still unclear. In a series of studies on apatite scintillators, the optical and scintillation properties of $(Gd_{0.4}Lu_{0.6})_8Sr_2(SiO_4)_6O_2$ crystals with different Ce doping concentrations were investigated.

2. Materials and Methods

The sample materials were synthesized by the floating zone (FZ) method using the same procedures as described in previous works,[62–66] and the Ce concentrations were 0, 0.001, 0.005, 0.01, and 0.02 with respect to Lu in the above chemical formula. After the preparation of the samples, X-ray diffraction (XRD) analyses were carried out using an X-ray diffractometer (Miniflex600, Rigaku) in the 2θ range of 20–60 deg.

A photoluminescence (PL) excitation and emission contour graph, in addition to PL *QY*, was obtained using Quantaurus-QY (Hamamatsu). PL decay time was evaluated using Quantaurus-τ (Hamamatsu), and the excitation and monitoring wavelengths were 340 and 425 nm, respectively. X-ray-induced scintillation spectra, decay curves, and afterglow profiles were obtained using our original setups.[67,68] To determine the scintillation *LY*, our typical setup for the pulse height spectrum (PHS) was used,[69] and the irradiation source was an ^{241}Am α-ray source. Although we challenged ourselves to measure the ^{137}Cs γ-ray-irradiated PHS, no clear photoabsorption peak was observed. Thus, we used an ^{241}Am source instead of ^{137}Cs. X-ray-induced afterglow profiles were determined using our original setup,[68] and the afterglow *A* was expressed as $100 \times (I_2 - I_0) / (I_1 - I_0)$, where I_0, I_1, and I_2 represent the signal intensity before X-ray irradiation (time $t = 0$, average of 150 data points), the signal intensity at $t = 2.5$ ms (average of 150 data points), and the signal intensity at $t = 20$ ms after X-ray off, respectively.

3. Results and Discussion

Figure 1 shows a picture of the as-grown samples. The as-grown samples appeared white-opaque owing to many cracks, and when the Ce concentration reached more than 1.0%, the color slightly changed to yellow, possibly owing to the absorption of Ce^{3+} ions. We crushed the as-grown sample rods to select a relatively transparent part for characterizations. In our experience, higher crystallinity can be achieved when the average ionic radius of the RE site is large,[62–66] and the current result follows this tendency: the 2.0% Ce-doped sample had more transparent parts than the other samples, since Ce^{3+} has a larger ionic radius than Lu^{3+}. Figure 2 shows the

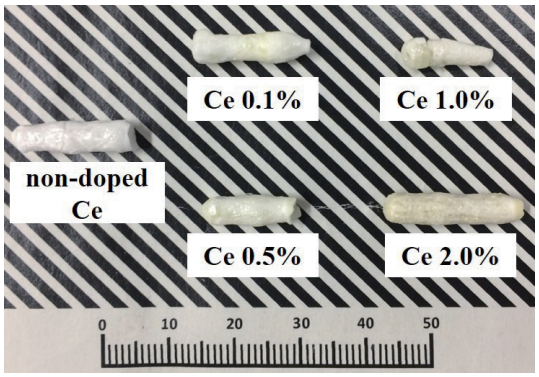

Fig. 1. (Color online) Appearance of as-grown crystalline samples.

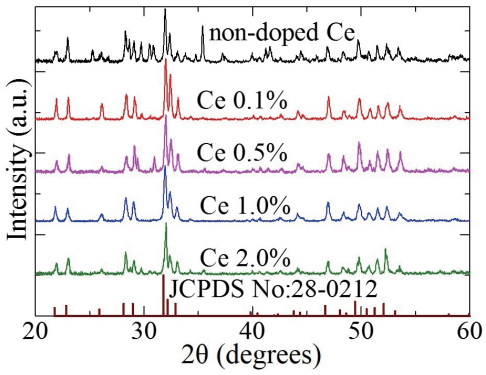

Fig. 2. (Color online) XRD patterns of samples and reference (JCPDS 28-0212).

XRD patterns of the present samples. For this characterization, some of the as-grown sample rods were crushed to powder form. In the non-doped sample, some unidentified peaks relative to the reference were observed in the 2θ range of 25–35 deg, and similar diffraction peaks were observed in the Gd_2SiO_5[70] and Lu_2SiO_5[71] phases. In the Ce-doped samples, no impurity phases were detected, or the amount largely decreased. This result is in line with our previous experiences on apatite scintillators.[62–66]

Figure 3 shows PL excitation and emission contour graphs of the non-doped and 0.5% Ce-doped samples. Since the spectroscopic features were similar in Ce-doped samples, we selected the 0.5% Ce-doped one as a representative. In the non-doped one, no significant emission was observed, whereas the 0.5% Ce-doped one exhibited a broad emission band from 380 to 650 nm upon 270–350 nm excitation. The signal-like structure at around 300 nm of the non-doped one would be due to an artifact. The PL *QY*s accumulated in the whole emission band of 0.1, 0.5, 1.0, and 2.0% Ce-doped ones were 2.7, 2.7, 3.8, and 1.4%, respectively. Figure 4 shows PL decay curves monitored at 425 nm upon 340 nm excitation. All the samples showed a similar decay shape, and they were approximated with the sum of two exponential functions assuming an instrumental response and the main emission. The decay time of the main component was 27 ± 1 ns for all the samples regardless of Ce concentration. This decay time is typical for Ce-doped oxide, and the PL emission origin is ascribed to the 5d–4f transition of Ce^{3+}. The emission of the non-doped one was unclear. One possibility was the unexpected contamination of Ce^{3+} below the detection limit of the PL measurement, and the other possibility was the host emission since such emission overlapped with this wavelength range, as described later.

Figure 5 shows X-ray-induced scintillation spectra of the present samples. All the samples showed a broad emission band from 350 to 700 nm. The sharp peak at 310 nm in the non-doped sample was ascribed to the 4f–4f transition of Gd^{3+}. When we doped Ce, the emission line of Gd^{3+} overlapped with the excitation bands of Ce^{3+} (Fig. 3), so this line was only observed in the non-doped one. Although the non-doped sample did not contain Ce in nominal composition and showed a detectable emission in PL (Fig. 3), an emission band from 350 to 700 nm was observed,

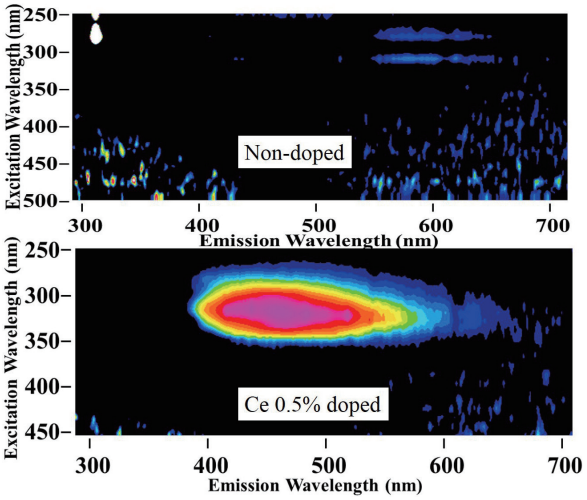

Fig. 3. (Color online) PL excitation and emission contour graphs of non-doped (top) and 0.5% Ce-doped samples. The horizontal and vertical axes show emission and excitation wavelengths, respectively.

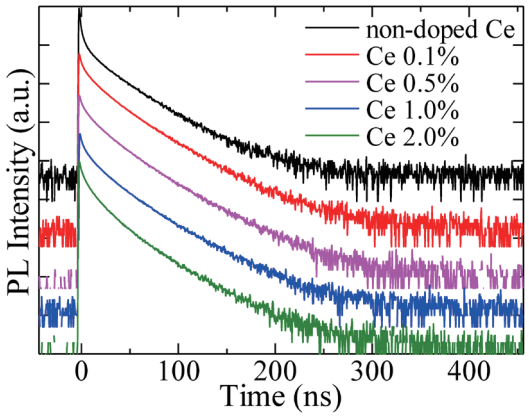

Fig. 4. (Color online) PL decay curves monitored at 425 nm upon 340 nm excitation.

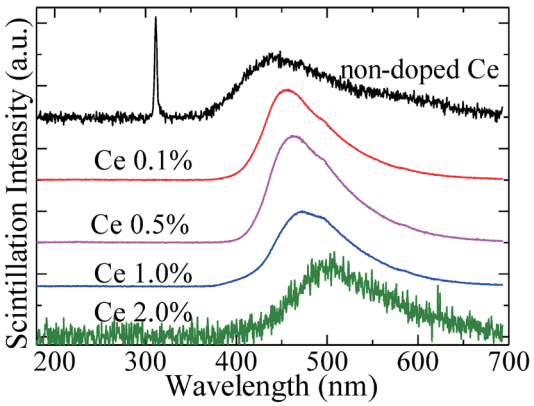

Fig. 5. (Color online) X-ray-induced scintillation spectra of present samples.

and the interpretation was the same as that of PL. In Ce-doped samples, a redshift of the emission band appeared, and it was blamed for the geometry of the setup. In this experiment, the geometry was of the transmission type, so the self-absorption affected the shapes of the spectra. Figure 6 shows the X-ray-induced scintillation decay curves of the samples. When we neglect the contribution from the excitation pulse, the decay time of the main component of the non-doped one was 32 ns. On the other hand, the main components in the decay curves of the Ce-doped samples were approximated from the sum of two exponential functions, and the decay times of the 0.1, 0.5, 1.0, and 2.0% Ce-doped ones were 19 + 58, 16 + 60, 17 + 46, and 15 + 164 ns, respectively. The explicit determination of the origins of each component is difficult, and we can propose several scenarios. One explanation is that the faster component would be due to the host emission quenched by the absorption of Ce^{3+}, and the slower component would come from Ce^{3+}.

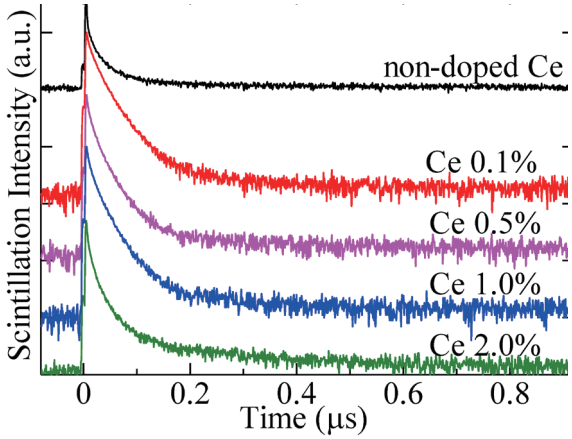

Fig. 6. (Color online) X-ray-induced scintillation decay curves of present samples.

The other possibility is that these two components both come from Ce^{3+} at different sites (Gd^{3+}, Lu^{3+}, and Sr^{2+} are possible), and some marginal emission of them would also be possible. The ionic radii of Ce^{3+}, Gd^{3+}, Lu^{3+}, and Sr^{2+} were 1.21, 1.14, ~1.04, and 1.35 Å, respectively. Although we could find the ionic radii of Ce^{3+}, Gd^{3+}, and Sr^{2+} from a previous work,[72] clear data of Lu^{3+} were not found, and we estimated the radius of Lu^{3+} from the other rare-earth ions.[73] Ce^{3+} would be able to substitute these sites from results of other common Ce-doped phosphors containing Gd^{3+}, Lu^{3+}, or Sr^{2+} ions as a host. On the other hand, the slowest component of 164 ns in the 2.0% Ce-doped sample would be affected by self-absorption, as evidenced by a huge redshift observed in Fig. 5.

Figure 7 shows the ^{241}Am α-ray-irradiated PHS of the present samples. The 0.5 and 1.0% Ce-doped ones showed a full-energy deposited peak structure at 125 and 300 ch, respectively. The scintillation *LY*s of the 0.5 and 1.0% Ce-doped ones were ~230 and ~620 ph/5.5 MeV-α, respectively. Although the 0.1% Ce-doped one showed a detectable signal, no clear peak was observed, and the determination of *LY* was difficult. The PHSs of the non-doped and 2% Ce-doped ones were close to a background level, and their scintillation *LY*s were very low. The reason for the low scintillation *LY* of the Ce-doped apatite materials is unclear, and in terms of conventional models,[58–61] the low PL *QY* and low energy migration efficiency from the host to emission centers are responsible for the low *LY*. Interestingly, a very recent work has revealed that the Tb-doped apatite shows a very high scintillation *LY*,[66] and the matching of the ionic radius of the dopant with the substitution site may be important in apatite families since the ionic radius of Tb^{3+} is quite close to that of Gd^{3+}. If this hypothesis is true, the doping of rare-earth ions between Gd^{3+} and Lu^{3+} (Tb^{3+}~Yb^{3+}) will be interesting.

Afterglow profiles of the current samples are shown in Fig. 8. When we put more Ce, the afterglow intensity decreased. The afterglow is thermally stimulated luminescence at room temperature caused by shallow traps.[74,75] In most cases, shallow traps are due to some types of defect, and the reduction in afterglow intensity in proportion to the Ce concentration is consistent with the crystalline quality, as shown in the results of crystal growth and XRD.

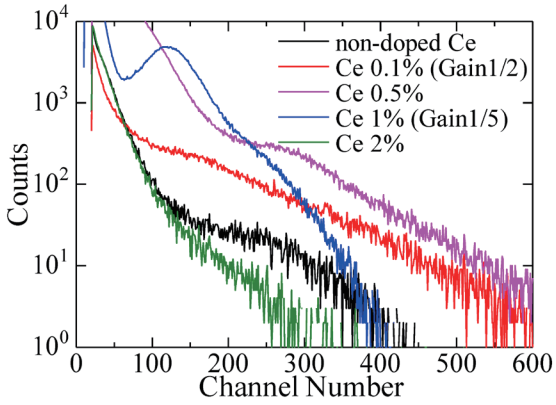

Fig. 7. (Color online) ^{241}Am α-ray-irradiated PHS of present samples.

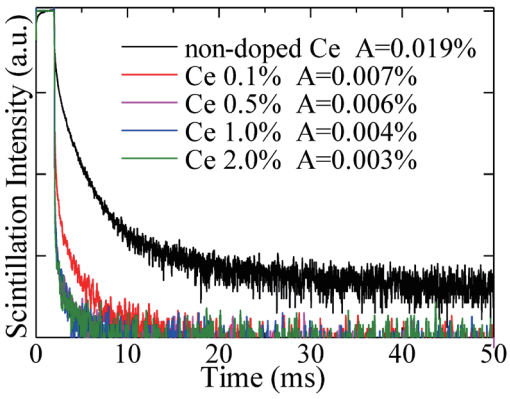

Fig. 8. (Color online) X-ray-induced afterglow profiles of present samples.

4. Conclusions

Non-doped and 0.1, 0.5, 1.0, and 2.0% Ce-doped $(Gd_{0.4}Lu_{0.6})_8Sr_2(SiO_4)_6O_2$ crystals were synthesized by the FZ method. In PL, an emission due to 5d–4f transitions of Ce^{3+} was observed at 380–650 nm with a decay time of 27 ± 1 ns in the Ce-doped samples. In X-ray-induced scintillation, similar spectral features were observed in Ce-doped ones, and a broad emission band was detected in the non-doped one. When ^{241}Am α-rays were irradiated, the scintillation *LY*s of the 0.5 and 1.0% Ce-doped samples were ~230 and ~620 ph/5.5 MeV-α, respectively.

Acknowledgments

This work was supported by Grants-in-Aid for Scientific Research B (19H03533, 21H03733, and 21H03736) and Early-Career Scientists (20K15026 and 20K20104) from the Japan Society for the Promotion of Science. The Cooperative Research Project of the Research Center for Biomedical Engineering is also acknowledged.

References

1 C. Kim, W. Lee, A. Melis, A. Elmughrabi, K. Lee, C. Park, and J. Yeom: Crystals **11** (2021) 669.
2 P. Dorenbos: Opt. Mater. X **1** (2019) 100021.
3 T. Yanagida: Proc. Japan Academy, B **94** (2018) 75.
4 G. F. Knoll: Radiation Detection and Measurement (Wiley, New York, 2010) 4th ed.
5 V. M. Sklyarchuk, V. A. Gnatyuk, and T. Aoki: Nucl. Instrum. Methods Phys. Res., Sect. A **953** (2020) 163224.
6 M. Koshimizu, Y. Muroya, S. Yamashita, M. Nogami, K. Hitomi, Y. Fujimoto, and K. Asai: Sens. Mater. **32** (2020) 1445.
7 K. Watanabe, K. Matsumoto, A. Unitani, K. Hitomi, M. Nogami, and W. Kockelmann: Sens. Mater., **32** (2020) 1435.
8 M. Nogami, K. Hitomi, T. Onodera, K. Matsumoto, K. Watanabe, A. Terakawa, and K. Ishii: Nucl. Instrum. Methods. Phys. Res., Sect. B **477** (2020) 43.
9 S. Yamamoto and H. Nitta: Nucl. Instrum. Methods Phys. Res., Sect. A **900** (2018) 25.
10 J. Glodo, Y. Wang, R. Shawgo, C. Brecher, R. H. Hawrami, J. Tower, and K. S. Shah: Phys. Procedia **90** (2017) 285.

11 K. Watanabe, T. Yanagida, K. Fukuda, A. Koike, T. Aoki, and A. Uritani: Sens. Mater. **27** (2015) 269.
12 T. Matsubara, T. Yanagida, N. Kawaguchi, T. Nakano, J. Yoshimoto, M. Sezaki, H. Takizawa, S. Tsunoda, S. Horigane, S. Ueda, S. Takemoto-Kimura, H. Kandori, A. Yamanaka, and T. Yamashita: Nat. Commun. **12** (2021) 4478.
13 T. Yanagida, Y. Fujimoto, S. Kurosawa, K. Kamada, H. Takahashi, Y. Fukazawa, M. Nikl, and V. Chani: Jpn. J. Appl. Phys. **52** (2013) 076401.
14 H. Takahashi, T. Yanagida, D. Kasama, T. Ito, M. Kokubun, K. Makishima, T. Yanagitani, H. Yagi, T. Shigeta, and T. Ito: IEEE Trans. Nucl. Sci. **53** (2006) 2404.
15 A. Horimoto, N. Kawano, D. Nakauchi, H. Kimura, M. Akatsuka, and T. Yanagida: Sens. Mater. **32** (2020) 1395.
16 T. Yanagida, T. Kato, D. Nakauchi, G. Okada, and N. Kawaguchi: Appl. Phys. Exp. **14** (2021) 082006.
17 N. Kawano, M. Akatsuka, H. Kimura, D. Nakauchi, T. Kato, and T. Yanagida: J. Mater. Sci. Mater. Electron. **32** (2021) 12903.
18 T. Yanagida, G. Okada, T. Kato, D. Nakauchi, and S. Yanagida: Appl. Phys. Exp. **9** (2016) 042601.
19 D. Onoda, M. Akatsuka, N. Kawano, D. Nakauchi, T. Kato, N. Kawaguchi, and T. Yanagida: J. Materi. Sci. Mater. Electron. **31** (2020) 20798.
20 M. Koshimizu, N. Kawano, A. Kimura, S. Kurashima, M. Taguchi, Y. Fujimoto, and K. Asai: Sens. Mater. **33** (2021) 2137.
21 T. Yanagida1, M. Sakairi, T. Kato, D. Nakauchi, and N. Kawaguchi: Appl. Phys. Exp. **13** (2020) 016001.
22 W. Drozdowski, A. J. Wojtowicz, S. M. Kaczmarek, and M. Berkowski: Phys. B **405** (2010) 1647.
23 T. Yanagida, Y. Fujimoto, M. Arai, M. Koshimizu, T. Kato, D. Nakauchi, and N. Kawaguchi: Sens. Mater. **32** (2020) 1351.
24 T. Jomkaew, W. Chaiphaksa, K. Siengsanoh, P. Limkitjaroenporn, C. Kedkaew, H. J. Kim, S. Kothan, A. Prasatkhetragarn, and J. Kaewkhao: Radiat. Phys. Chem. **189** (2021) 109749.
25 T. Kato, G. Okada, K. Fukuda, and T. Yanagida: Radiat. Meas. **106** (2017) 140.
26 S. Alamdari, M. S. Ghamsari, and M. J. Tafreshi: Prog. Nucl. Energy **130** (2020) 103495.
27 T. Yanagida: Opt. Mat. **35** (2013) 1987.
28 Y. Fujimoto, D. Nakauchi, T. Yanagida, M. Koshimizu, and K. Asai: Sens. Mater. **33** (2021) 2147.
29 C. M. Combes, P. Dorenbos, C. W. E. van Eijk, K. W. Kramer, and H. U. Gudel: J. Lumin. **82** (1999) 299.
30 A. Ishikawa, A. Yamazaki, K. Watanabe, S. Yoshihashi, A. Uritani, Y. Sakurai, H. Tanaka, R. Ogawara, M. Suda, and T. Hamano: Sens. Mater. **32** (2020) 1489.
31 D. Shiratori, D. Nakauchi, T. Kato, N. Kawaguchi, and T. Yanagida: Sens. Mater. **32** (2020) 1365.
32 J. T. M. de Haas and P. Dorenbos: IEEE Trans. Nucl. Sci. **55** (2008) 1086.
33 T. Matsuo, T. Kato, H. Kimura, F. Nakamura, K. Hashimoto, D. Nakauchi, N. Kawaguchi, and T. Yanagida: J. Lumin. **231** (2020) 117803.
34 M. Moszynski, M. Kapusta, M. Mayhugh, D. Wolski, and S. O. Flyckt: IEEE Trans Nucl. Sci. **44** (1997) 1052.
35 N. Kawaguchi, H. Masai, M. Akatsuka, D. Nakauchi, T. Kato, and T. Yanagida: Sens. Mater. **33** (2021) 2215.
36 A. M. Srivastav: J. Lumin. **129** (2009) 1419.
37 P. Kantuptim, M. Akatsuka, D. Nakauchi, T. Kato, N. Kawaguchi, and T. Yanagida: Sens. Mater. **32** (2020) 1357.
38 Y. Wu and G. Ren: Opt. Mater. **35** (2013) 2146.
39 M. Akatsuka, H. Kimura, D. Onoda, D. Shiratori, D. Nakauchi, T. Kato, N. Kawaguchi, and T. Yanagida: Sens. Mater. **33** (2021) 2243.
40 T. Yanagida, Y. Fujimoto, H. Yagi, and T. Yanagitani: Opt. Mater. **36** (2014) 1044.
41 M. Yang, Y. Wu, J. Shi, H. Li, X. Zhao, and G. Ren: Radiat. Meas. **147** (2021) 106638.
42 H. Fukushima, M. Akatsuka, H. Kimura, D. Onoda, D. Shiratori, D. Nakauchi, T. Kato, N. Kawaguchi, and T. Yanagida: Sens. Mater. **33** (2021) 2235.
43 J. Hu, H. Guo, W. Du, F. Yang, Q. Yang, and H. Feng: Ceram. Int. **47** (2021) 28505.
44 D. Nakauchi, T. Kato, N. Kawaguchi, and T. Yanagida: Sens. Mater. **33** (2021) 2203.
45 C. Aarle, K. W. Krämer, and P. Dorenbos: J. Lumin. **238** (2021) 118257.
46 T. Yanagida, Y. Fujimoto, H. Masai, G. Okada, T. Kato, D. Nakauchi, and N. Kawaguchi: Sens. Mater. **33** (2021) 2179.
47 D. Rutstrom, L. Stand, B. Dryzhakov, M. Koschan, C. L. Melcher, and M. Zhuravleva: Opt. Mater. **110** (2020) 110536.
48 M. Akatsuka, D. Nakauchi, T. Kato, N. Kawaguchi, and T. Yanagida: Sens. Mater. **32** (2020) 1373.
49 V. Alizadeh, P. Hosseinkhani, M. Najafi, and M. Abdolahzadeh: J. Lumin. **233** (2021) 117885.
50 H. Kimura, T. Kato, D. Nakauchi, N. Kawaguchi, and T. Yanagida: Sens. Mater. **32** (2020) 1381.
51 J. Zhou, X. Liu, Y. Lai, Y. Chen, C. Qiu, and L. Lei: Opt. Mater. **107** (2020) 110152.

52 H. Masai, T. Ina, H. Kimura, N. Kawaguchi, and T. Yanagida: Sens. Mater. **33** (2021) 2155.
53 S. Hao, X. Liu, M. Gu, Q. Li, M. Huang, and H. Yang: J. Lumin. **240** (2021) 118449.
54 T. Kato, D. Nakauchi, N. Kawaguchi, and T. Yanagida: Sens. Mater. **32** (2020) 1411.
55 K. Higuchi, H. Arakawa, A. Matsumoto, K. Narita, and Y. Morioka: Appl. Radiat. Isotopes **175** (2021) 109797.
56 D. Nakauchi, T. Kato, N. Kawaguchi, and T. Yanagida: Sens. Mater. **32** (2020) 1389.
57 S. Yamamoto and H. Tomita: Appl. Radiat. Isotopes **168** (2021) 109527.
58 D. J. Robbins: J. Electrochem. Soc. **127** (1980) 2694.
59 A. Lempicki, A. J. Wojtowicz, and E. Berman: Nucl. Instrum. Methods Phys. Res., Sect. A **333** (1993) 304.
60 P. A. Rodnyi, P. Dorenbos, and C. W. E. van Eijk: Phys. Status Solidi C **187** (1995) 15.
61 P. Dorenbos: Nucl. Instrum. Methods Phys. Res., Sect. A **486** (2002) 208.
62 T. Igashira, M. Mori, G. Okada, N. Kawaguchi, and T. Yanagida: Opt. Mater. **64** (2017) 239.
63 T. Igashira, M. Mori, G. Okada, N. Kawaguchi, and T. Yanagida: J. Rare Earths **35** (2017) 1071.
64 T. Igashira, N. Kawano, G. Okada, N. Kawaguchi, and T. Yanagida: Optik **155** (2018) 36.
65 T. Igashira, N. Kawano, G. Okada, N. Kawaguchi, and T. Yanagida: Opt. Mater. **79** (2018) 232.
66 K. Watanabe, T. Yanagida, D. Nakauchi, and N. Kawaguchi: Jpn. J. Appl. Phys. **60** (2021) 106002.
67 T. Yanagida, K. Kamada, Y. Fujimoto, H. Yagi, and T. Yanagitani: Opt. Mater. **35** (2013) 2480.
68 T. Yanagida, Y. Fujimoto, T. Ito, K. Uchiyama, and K. Mori: Appl. Phys. Exp. **7** (2014) 18.
69 T. Yanagida, N. Kawaguchi, Y. Fujimoto, K. Fukuda, K. Watanabe, A. Yamazaki, and A. Uritani: J. Lumin. **144** (2013) 212.
70 R. K. Tamrakar and K. Upadhyay: Optik **127** (2016) 5204.
71 L. Fan, Y. Shi, J. Xu, J. Xie, and F. Lei: J. Mater. Res. **29** (2014) 2252.
72 Y. Ohgi: Crystal Growth, Crystal Structure and Optical Properties of Ce-doped Oxyapatite Single Crystals, Master thesis, Univ. of Tokyo (2009) (in Japanese).
73 R. D. Shannon: Acta Cryst. A**32** (1976) 751.
74 T. Yanagida, G. Okada, and N. Kawaguchi: J. Lumin. **207** (2019) 14.
75 T. Yanagida: J. Lumin. **169** (2016) 544.